
Article:
Caulkin, R, Islam, MS, Jia, X et al. (1 more author) (2014) Studies for the development of a virtual permeameter. Computers and Chemical Engineering, 68. 190 - 202. ISSN 0098-1354

https://doi.org/10.1016/j.compchemeng.2014.05.027

Studies for the Development of a Virtual Permeameter

Richard Caulkin*, Mishal S. Islam, Xiaodong Jia, Michael Fairweather

Institute of Particle Science and Engineering, School of Process, Environmental and Materials Engineering, University of Leeds, Leeds LS2 9JT, UK

*****Corresponding author: Dr. Richard Caulkin
Tel: +44 (0)1977 557021
Email: r.caulkin@gmail.com
Postal address: Institute of Particle Science and Engineering, School of Process, Environmental and Materials Engineering, University of Leeds, Leeds LS2 9JT, UK

Current address: 83 Stansfield Drive, Castleford, West Yorks, WF103DD, UK

Abstract
A systematic analysis on the use of the lattice Boltzmann method (LBM) for predicting the permeability of packed beds is presented. A filtration rig is used to obtain permeability measurements of beds of glass beads, sand and crushed minerals. Subsequently, X-ray micro-tomography is employed to image bed samples for use as input to LBM calculations. Uncertainties in accuracy and reliability of predictions arising from pixel resolution, sample size and digitisation errors in the simulations are evaluated through sensitivity studies and assessments of the representativeness of the bed samples. For beds of spherical and near-spherical particles, any bed sample is capable of providing reproducible and reliable simulation results provided that the particles are adequately resolved within an LBM simulation . For more complex beds of polymorphous, polydisperse particles estimation of the permeability of representative samples of the entire bed is required before average results comparable with data are obtained.

Keywords: Permeability; packed beds; lattice Boltzmann method; x-ray micro-tomography

1. Introduction

Filtration is widely used in many industries as a method of separation in processes such as distillation, absorption, drying and membrane separation, and also in dead-end filtration on which this paper is specifically focused. At present, one of the most common methods of predicting and analysing permeation through a filtration bed, and of designing new beds, is by utilising existing experimental data and empirical correlations in trial and error testing that is largely based on experience, rather than by using quantitative prediction methods and rigorous design rules. Much of existing data on filtration and sedimentation focuses on macro-scale phenomena, e.g. Zamani and Maini, 2009 and references therein. Little research has been documented regarding the use of micro-scale information gathered, for example, using X-ray micro-tomography (XMT), which can be subsequently coupled to more detailed simulation techniques, for example, based on the lattice Boltzmann method (LBM). Another common flaw in the traditional methods used for predicting filtration performance is in quantifying the phenomena through the use of porosity which, in itself, is not a sufficient parameter for characterising packed beds as varying bed tortuosities can have the same porosity; nevertheless, porosity is still widely used as the key parameter in describing macroscopic flow through a porous medium.

The work described in this paper is aimed at the development of fundamental understanding and, through the use of sensitivity analyses and porous media simulations, the creation of a virtual permeameter. It is conjectured that such understanding would enable the structure-flow relationships of bulk porous media to be assessed based on the micro-structural details of small samples and, ultimately, on the details of individual particles that make-up such structures. The study evaluates the feasibility of such an approach and establishes a routine for its implementation using XMT and LBM. Potential applications for a virtual permeameter include its use as a design tool in the development of new filters, and also in oil exploration where a core plug from a costly test drill is usually too small for its porosity to be measured sufficiently accurately using conventional experimental methods.

LBM excels as a method for simulating fluid flow in situations involving complex boundaries, such as flows through packed beds. Many works have been published which give detailed descriptions of LBM, and its precursors lattice gas automata and cellular automata techniques (Aidun and Lu, 1995; Martys and Chen, 1995; Wolf-Gladrow, 2000; Succi, 2001; Macnab et al., 2002; Sullivan et al., 2007; Dünweg and Ladd, 2009; Tafreshi et al., 2009), with an in-house version of LBM (DigiFlow) used in the present work (Caulkin et al., 2008). The method provides high levels of detail in flows with complex boundaries, is relatively straightforward to implement as a software program and is relatively easily parallelised to make the best use of today's computing facilities. In addition, it is lattice-based and thus can use digitally specified structures as direct input, no matter how complex those structures may be. Such structures can be obtained either from computer-based digital simulation techniques or through tomographic imaging techniques such as XMT.

Application of LBM has certain sensitivities, much like all computational fluid dynamic approaches. In terms of the present application, the sensitivities of LBM include errors associated with the accuracy of the digitisation of solid surfaces and volumes, and in particular particles, since the technique does not necessarily solve for all length and time scales associated with a flow. Additionally, and in terms of applying the technique to enable the structure-flow relationships of bulk porous media to be assessed based on the details of small samples, the representativeness of the sample itself is of crucial importance. In regard to these issues, although permeation is widely used in other fields such as geophysics to measure permeability through strata, and XMT has been used to aid the analysis of permeability through rock (Arns et al., 2004) and to validate it as a suitable measurement technique (Wildenshild et al., 2002), there has been little work reported on the errors associated with the digitisation of particles and beds within LBM simulations.

Previous work by Vidal et al. (2009) assumed that packed beds of polymorphous structures could be represented by spherical particles for the purposes of their LBM simulations, with results compared against predictions of the Carman-Kozeny equation (McCabe et al., 2005) to validate this assumption. As far as the present authors are aware, little other work has been performed to directly validate whether such polymorphous structures, especially those made up of rods or the amorphous particles found in minerals, can be considered spherical for the purposes of LBM simulation. Vidal et al. (2009) considered packing compression of a bed, and the errors associated with the size of particles in the bed, i.e. digitisation errors, but related errors in permeability to the ratio between the mean sphere diameter and the lattice spacing, rather than considering the resolution of individual particles. Additionally, this work considered errors in terms of the volume of the bed as a whole, rather than its specific dimensions. It was concluded (Vidal et al., 2009) that there was a 30-40% error between LBM predictions of permeability and experimental data, with the predictions found to follow the Carman-Kozeny equation, but with an increasing deviation observed towards lower predicted permeability values. In earlier work Clague and Phillips (1997) used LBM to calculate the permeability of beds of fibrous material, using the Brinkman screening length (Koch et al., 1998) to ensure that the bed size employed in the simulations was sufficiently large to give accurate predictions. These authors therefore considered the sample size required in any simulation, although the study was specific to fibrous material. Stockman (1999) also discussed digitisation errors associated with flow through an ideal cubic array of spheres, acknowledging the error although not investigating it further.

The present work utilises a systematic approach to investigate prediction of the permeability of packed beds made up of mono-disperse spherical particles. The impact of discretisation and XMT errors at a particle level on the accuracy of LBM simulations is investigated. The work described also considers the minimum digitisation requirements for individual particles within a bed, and the dimensions (rather than the volume) of the sample from a bed required to give reliable predictions of permeability. The influence of the region of the larger bed from which the sample is taken is also considered. Using the same principles, the work is then extended to include beds made up of mono-disperse, near-spherical sand particles, and of polydisperse, polymorphous particles.

2. Experimental and predictive approaches

2.1 Bed formation and filtration experiments

The permeability was obtained experimentally through the use of a single-run, pressure regulating filtration rig (Fig. 1). To measure the size of particles used to make up the beds, a Malvern Mastersizer 2000 using a Hydro S cell (50-120 ml volume) was employed with de-ionised water as the dispersant. Spherical glass particles were sized using D[4,3], i.e. the volume moment mean of the particle, with particles of a mean diameter of 116 μm and a narrow particle size distribution used in this work. Beds made up of mono-disperse sand particles, and of polydisperse, polymorphous particles, are considered later, although these contained sand grains with a narrow size range and a mean diameter of 236 μm, and a random selection of particles of non-uniform shape and sizes ranging from 115 μm to 375 μm, respectively.

[FIGURE 1]

The beds were formed by thoroughly washing the particles beforehand; twice with tap water and a third time with distilled water. A mass of 45 g of particles was added to 200 ml of distilled water and 15 g of salt and mixed vigorously and thoroughly. Particles were subsequently placed in a vacuum oven (at 25 ^{o}C) for 0.5 hr to remove trapped air. Once void of bubbles, the mixture was introduced into a steel filtration rig which consisted of a steel tube with an inner diameter of 40 mm. The sample solution was mixed once more in the cylinder before being allowed to settle to ensure any air voids were expelled. The bottom end

of the tube screwed into a sieve filtration attachment that allowed the flow of water through it but not the particles, and hence the formation of a particulate bed (Fig. 2). To account for water resistance from the sieve as well as the effect of gravity on the water column, an experimental run was performed under gravity with a sieve but without a bed. This contribution was then subtracted from the measurements made with the bed present to ensure that the flow rate recorded was purely for the pressure-driven flow through the porous medium. The upper end of the tube was screwed into a pressure regulating unit, which in turn was connected to an outside pressure pump with a 4 bar output. A PC adjacent to the rig measured mass flow rate using the weight of water output as a function of time. Converting mass to volume flow rate, the permeability, k, was calculated from:

$$k = U\mu/(\Delta P/H) \quad (1)$$

where U is the velocity (cm s^{-1}), μ is the dynamic viscosity (0.00909 g cm^{-1} s^{-1}), ΔP is the pressure difference (e.g. 1.5 bar ≈ 15.2×10^5 g cm^{-1} s^{-2} in the case of the sensitivity studies described below), and H is the height of the bed (≈4 cm).

[FIGURE 2]

Each experiment was run at least eight times to ensure stable and statistically acceptable results with runs repeated until stability was reached. The data were averaged and the mass flow rate used as the basis for comparisons with LBM predictions.

Below is a list of errors associated with the experimental procedure, together with their assessed quantitative error value:

- Analogue gauge pressure used producing less precise readings than digital. This includes a visual approximation, e.g. 1.5 bar ~ 1.45-1.55 bar ≈ ±3.5% error.
- Pressure alters between the start of an experiment and its completion due to the compressibility of the volume of air inside the steel tube, with compressible air replacing incompressible liquid with time. This implies errors towards the end of an experiment that are not there just after steady flow is obtained (roughly 1 s after initiation). However, the compression of air under pressure would be consistent across all experiments, and so deviations of pressure due to air compression would be negligible.
- Ambient pressure is assumed to be 1 atm, although this value can alter. A higher experimental pressure reduces such errors, and the overall effect on the experiments was judged to be negligible.
- Liquid loss of approximately 15 g occurred over the course of an experimental run from spillage/leakage. However, this only affects the end weight and, although there is roughly an 8% error in weight from the start to finish of an experiment, there is no resulting error in the flow rate.
- Possible blockage of the support mesh by the particles could have reduced the flow rate, although the variation between each experiment was judged to be negligible. The error between an ideal experiment and the current method was also examined in sensitivity studies carried out using LBM simulations, with this error discounted as insignificant as a consequence.
- Slight density fluctuations between each experimental run could have occurred due to the evaporation of water. This is particularly relevant in summer since runs can last several hours, with the salinity of the solution gradually increasing over the course of an experiment as a consequence. A difference of 0.1 g leads to a 0.2 % error in the derived flow velocity.
- Attempts were made to keep the temperature of the laboratory, and hence the fluid, constant as changes would affect the viscosity.

Although there are areas of potential error in the experiments, as related to the ideal experimental setup, the errors differentiating the current experimental procedure and industrial practice are much smaller. Overall, the range of error from all the sources noted above was considered to be a maximum of ±12-15%. Much of this error was generated by visual failings resulting in the rounding-off of gauge pressure readings. The bulk of the remaining error is due to evaporation of the water as the experiments progressed, and also changes in viscosity due to variations in temperature.

2.2 X-ray micro-tomography

XMT is a non-destructive, non-invasive imaging method that is relatively fast and can give good levels of structural detail. However, the equipment is expensive, and in common with many other imaging techniques, the edges of scanned structures can be blurred. Scanned images can also result in non-uniform shades, e.g. due to beam hardening, and the saved structures are subject to threshold errors. The structural information concerning the particle beds required for the LBM simulations was obtained in this work using a Phoenix Nanotom XMT machine to take three dimensional scans of bed samples. The Nanotom is a 160-kV nanofocus CT scanner, equipped with a 5-megapixel (2304×2304 pixels) CCD detector which is capable of achieving a maximum pixel resolution of better than 0.5 μm. The largest sample size the scanner can accommodate is approximately 60 mm in width.

Experimental bed samples were dried in an oven (60 ^{o}C overnight) until they solidified before being removed from the steel cylinder of the filtration rig. An approximately 8×8×8 mm sample was cut from the larger packed bed for measurement. Scanning of the sample took approximately 0.5 hr; however, the time for reconstruction of the sample was dependant on the number of computers used and the specific size of the sample to be reconstructed. In this work, the terms pixel, voxel and lattice unit (LU) are used interchangeably. Voxel length or lattice unit, where one lattice unit is equivalent to one voxel, are used as opposed to physical length measurements (i.e. μm) to simplify relating the XMT data to LBM dimensionless units.

The samples were scanned with ×25 magnification, or 2μm pixel^{-1} resolution, 1500 projections, 100 kV and 100 μA. Typically, a 300x300x300 sample took approximately 15-20 mins for reconstruction running on a 4-PC cluster with a total of 8 GB of RAM.

2.3 Lattice Boltzmann method

In recent years LBM has been increasingly used to predict the permeability of porous media such as packed beds and flows in other complex geometries, largely due to the simplicity with which complex structures and wall boundaries can be represented.

Unlike most other computational fluid dynamic approaches to predicting fluid flow, which are based on the continuum assumption, LBM uses a gas-kinetic approach to simulate the mechanics of the fluid system. It assumes that, in each grid cell used in the simulation, fluid is composed of a fixed number of discrete fluid particles, each being described by a density distribution function and a fixed velocity. Discrete time steps are used to simulate collisions between the particles, with the rules that dictate these collisions ensuring that the time-averaged motion of the particles is consistent with the Navier-Stokes equations.

The standard lattice Boltzmann equation with the Bhatnagar-Gross-Krook (BGK) collision operator (Bhatnagar et al., 1954) can be written as (Qian et al., 1992):

$$f_\alpha(\boldsymbol{x} + \boldsymbol{c}_\alpha \delta t, t + \delta t) = f_\alpha(\boldsymbol{x}, t) - \frac{1}{\tau}\left[f_\alpha(\boldsymbol{x}, t) - f_\alpha^{eq}(\boldsymbol{x}, t)\right] \text{ with } \alpha = 0, 1, 2, \ldots N \quad (2)$$

where **x** is the position in space, t is time, δt and $\boldsymbol{c}_\alpha \delta t$ are time and space increments, f_α is the particle density distribution function in the α direction, f_α^{eq} is the corresponding equilibrium distribution function, $\mathbf{c}_\alpha$ is the particle velocity in the α direction, τ is the single relaxation time and N the number of discrete particle velocities. Most forms of the lattice Boltzmann equation are solved in two steps: collision and streaming. During collision, the particle velocity distribution function in each direction is relaxed toward a quasi-equilibrium distribution, whilst in the streaming step the distributions are moved to the adjacent nodes.

DigiFlow (Caulkin et al., 2008), the in-house LBM code employed in this work, uses the BGK method with a D3Q19 lattice and periodic boundary conditions. Calculations are performed in a three-dimensional volume with N = 19. The equilibrium distribution for this discrete set of lattice velocities is given by (Qian et al., 1992):

$$f_\alpha^{eq} = w_\alpha \rho \left[1 - \frac{3}{2}\frac{\boldsymbol{u}^2}{c^2}\right] \text{ for the rest particle } \alpha = 0$$
$$f_\alpha^{eq} = w_\alpha \rho \left[1 + 3\frac{\boldsymbol{c}_\alpha \cdot \boldsymbol{u}}{c^2} + \frac{9}{2}\frac{(\boldsymbol{c}_\alpha \cdot \boldsymbol{u})^2}{c^4} - \frac{3}{2}\frac{\boldsymbol{u}^2}{c^2}\right] \text{ for particle } \alpha = 1,\ldots,18 \quad (3)$$

where

$$w_0 = \frac{1}{3}, \quad w_{1,\ldots,6} = \frac{1}{18}, \quad w_{7,\ldots,18} = \frac{1}{36}$$

$$\boldsymbol{c}_\alpha = \begin{cases} (0,0,0)c & \alpha = 0 \\ (\pm 1,0,0)c, (0,\pm 1,0)c, (0,0,\pm 1)c & \alpha = 1,\ldots,6 \\ (\pm 1,\pm 1,0)c, (\pm 1,0,\pm 1)c, (0,\pm 1,\pm 1)c & \alpha = 7,\ldots,18 \end{cases}$$

$$\text{and } \rho = \sum_\alpha f_\alpha \qquad \rho \boldsymbol{u} = \sum_\alpha f_\alpha \boldsymbol{c}_\alpha \qquad v = \frac{2\tau - 1}{6} \quad (4)$$

where ρ and **u** are the macroscopic fluid density and velocity, w_a is a weighting factor, c is the speed of sound (=1/√3), and v is the kinematic shear viscosity.

The DigiFlow software implements the simple bounce-back scheme for the no-slip wall boundary condition on the surfaces within the flow. Also, the flow is driven by a constant body force, f_b, equivalent to a constant pressure gradient through the bed, such that:

$$f_b = \Delta P / H \quad (5)$$

$$k = \frac{U_s v}{f_b} \quad (6)$$

where U_s is the superficial velocity, and f_b has units MU LU^{-2} δt^{-2} (where MU is mass units).

2.4 Carman-Kozeny equation

Permeability is superior to porosity when used in describing fluid flow through the complex porous structures of a packed bed as it describes porosity with respect to, amongst other things, the particle diameter. A widely used empirical formula for predicting the permeability of packed beds is the Carman-Kozeny equation (McCabe et al., 2005). It is defined as:

$$k = -\frac{U_s \mu}{\nabla p} = \frac{D^2 \varepsilon^3}{180(1-\varepsilon)^2} \quad (7)$$

where D is the particle diameter and ε the porosity. This equation states that the permeability scales linearly with the hydraulic radius squared, leaving one undetermined parameter, the Kozeny constant, whose value is found experimentally to be close to 5.

A number of experimental and numerical studies have demonstrated that the Carman-Kozeny equation yields reasonably accurate predictions of permeability (within 5-10 %) for porosities <0.5. These include mono-disperse, randomly packed beds of spherical particles (Klemm et al., 2001; Thies-Weese and Phillipse, 2004), periodic arrays of spheres (Muhammad, 1995) and fractal porous media and polydispearse arrangements (Adler, 1988; Stanley and Andrade, 2001).

3. Results and discussion

Two major sources of simulation error for fluid flow through a packed bed (using the methodology described) are associated with the accuracy of digitisation of the particles within a bed, and errors arising from the representativeness of the specific bed sample used as the basis of the XMT scans. The likely magnitude of errors within a given simulation, and the means of reducing them to acceptable levels, is considered through sensitivity analyses with all variables fixed apart from the one under scrutiny. These issues are considered below through a number of sphere-in-channel benchmark tests (Section 3.1) and in porous media simulations (Section 3.2) of the bed types investigated. In all cases, inflow and outflow periodic boundary conditions were utilised in the calculations.

It is customary in LBM calculations to express length related parameters in lattice units (LU), and volume in terms of voxels. A voxel is the smallest building block in the shape of a cube, having a physical volume of L^3 where L is the linear size of the cube, equal in value to the pixel resolution used. For area, the units used are pixels, where a pixel represents a single face of the cube, having a physical area of L^2. Length is then in pixels, with one pixel equivalent to one length unit, L.

3.1 Sphere-in-channel benchmark tests

In investigating the effect of particle resolution, focus was placed on consideration of flow round a spherical particle in a square channel. The first test case considered, with increasing resolution of the sphere shape at constant resolution of the flow, focused on the representation of the spherical surface. The second test case explored the effect of both flow and sphere resolution at the same time. The Reynolds number used in both sets of benchmark simulations ranged from 0.16 to 0.28.

In the first test case, errors arising from the size and digital representation of simulated spherical particles were determined by defining a square duct with a cross-sectional area of 160×160 LU and a length of 384 LU. Seven increasingly accurate digital representations of a sphere with a constant physical diameter were embedded into the centre of the square duct and flow past the object simulated. The shape of each sphere was created using digital building software to generate spheres with diameters of 2, 4, 8, 16, 32, 64 and 128 pixels, examples of which are shown in Fig. 3. Each digital representation was stretched to the same size as the 128 pixel diameter case to ensure that wall effects would be approximately constant with increasing resolution. The duct dimensions were selected so that the spheres occupied 80% of the cross-sectional diameter and 1/3 of the duct length. Naturally, a 2 pixel diameter sphere is in fact a cube, and 4 and 8 pixel diameter spheres are more cruciform than spherical. For this flow, and from the equation for the permeability with a constant f_b, Eq. (6), the superficial velocity, U_s, is the only variable.

[FIGURE 3]

The results are given in Fig. 4, where S_d is the spherical particle diameter (pixels). The rise in permeability observed when the sphere representation is increased from 2 to 4 pixels is due to its drastic change in shape (from cubic to cruciform). The addition of a further 4 pixels to the diameter results in a slight decrease in permeability due to the additional pixels placed near the centre of the cross-shaped sphere increasing frictional effects. Beyond this point, further

refinement of the sphere representation results in a rapid asymptoting of the predicted permeability, with an essentially constant permeability reached by 64 LU.

[FIGURE 4]

An alternate method of assessing the error arising from the degree of pixilation, examined in the second test case, is to keep the ratio of the sphere diameter to duct width constant, and to alter the complexity of the sphere by increasing the number of representative voxels. As the size of the sphere increases, and the sphericity of the particle improves, the duct cross-sectional area and length are also increased. These calculations began with a sphere diameter of 8 pixels, and increased incrementally by 2 pixels to 32 pixels, with 48 and 64 pixel diameter calculations also performed. Whereas the first set of simulations noted above kept wall effects approximately constant, this second case gradually distances the sphere from the walls of the duct, thereby reducing such effects. Calculations using low pixel values resulted in large errors in the predicted permeability, with reduced error for more accurate digital representations of the sphere, as indicated by the volume-based digitisation error in Fig. 5. In our model, particle shape is represented using cohesive collections of pixels. Therefore volume based digitisation error (%) is defined as: (volume_of_digital_version / analytical_volume_of_the_object - 1)*100. The error associated with the predicted permeability correlates well with the results of Fig. 4, with both sets of data confirming that sphere diameters of 16 and 32 pixels ensure an error, relative to asymptotic permeability values (i.e. that obtained using a sphere diameter of 128 pixels), of approximately 14.5% and 6%, respectively (Table 1).

Exploring the effect of flow and sphere resolution at the same time, the predictions of Fig. 6 indicate a decrease in the superficial velocity, corresponding with increases in the permeability (Fig. 5), with this velocity approaching an approximately constant value as particle size increases. This is likely due to the increasing resolution used in the computations, with the 122.5 k nodes used in calculations for the smallest sphere comparing with 48.02 M nodes employed for the largest.

[FIGURE 5]
[TABLE 1]
[FIGURE 6]

3.2 Porous media simulations

In Section 3.1, spheres were used to test the required numerical resolution in single particle benchmark tests. This section builds on that work, examining packed arrays of particles studied using XMT. Following sensitivity studies to determine suitable volumes and dimensions of samples taken from a larger bed, investigations of the flow through sphere packed beds are reported for a range of drive pressures using samples taken from different locations within a larger bed. The same principles are then applied in examining beds of non-spherical particles to assess whether the conclusions reached for spherical particle beds remain valid.

3.2.1 Sensitivity studies for spherical particle beds

The Brinkman screening length is defined as the length scale over which velocity disturbances caused by individual cylindrical fibres decay to the bulk fluid velocity, and is simply stated as $\sqrt{k}$, where k is the hydraulic permeability. A simulation domain 14 times greater than the Brinkman length is sufficiently large to smooth out the effect of local inhomogeneities (Clague and Phillips, 1997). For beds packed with spherical particles, there is no theoretical method of determining the minimum size of sample required to be statistically representative of the permeability of the larger bed. The Brinkman length does not correlate well for spheres, as in the following example: using a cm scale, a sphere of diameter 0.0116 and a porosity of 0.4, from the Carman-Kozeny equation, has a permeability

of 1.34×10^{-7}. Thus, according to the Brinkman screening length approach, the minimum length necessary is 0.0051 cm (i.e. 14×0.00037 cm) or, at 2μm/pixel resolution, 26×26×26 which is clearly unsatisfactory. In the studies reported below, the minimum bed dimensions considered in the sensitivity analysis are 100×100×100.

A series of simulations were performed based on XMT scans of varying sizes of sections of a packed bed with, on average, 58 pixels used across the diameter of each particle, i.e. larger than the minimum representation, as determined from the work reported in Section 3.1, required to ensure that errors arising from sphere representation were minimised.

[FIGURE 7]

Figure 7 demonstrates how increasing the sample volume influences the predicted permeability. The results show a clear distinction between sample volumes roughly less than and greater than 10^7 LU^3, with larger volumes displaying an approximately constant permeability. However, these results could be misleading, being based on volume alone, since the length and cross-sectional area of the sample may be influential. Clearly, therefore, a sample with a small cross-sectional area and a large length would not produce predictions of permeability and superficial velocity equal to those of a sample with a larger cross-sectional area and shorter length; consequently, it is necessary to assess the impact on predictions of varying the cross-sectional area of a sample of a fixed length, and of varying the sample length for a fixed cross-sectional area. Additionally, the location within the larger bed from which the sample is taken requires investigation.

Comparisons were made between LBM predictions, and those of the Carman-Kozeny equation, and measurements of permeability for the bed as a whole. Simulations were conducted for bed sample lengths of 100, 200, 300, 400 and 600 LU, with sample cross-sections of 100, 200, 300, 400 and 600 LU^2. Results for a fixed sample length of 600 LU with varying cross-section, and a fixed cross-section of 300 LU^2 and varying length, are considered below. Other combinations are excluded since samples with a cross-sectional area of 300 LU^2 gave results that were negligibly different from those obtained from larger cross-sections, denoting convergence in the results with sample size. The use of a fixed length of 600 LU with varying cross-sections also serves to highlight the influence of the latter on predicted permeabilities. Equivalent results obtained with a fixed length of 300 LU were again little different from those predicted using 600 LU length samples, although use of the latter sample length allows errors arising from too small a cross-section to be more readily identified.

[FIGURE 8]

In undertaking these calculations, simulation stability was assured by fixing $f_b = 10^{-4}$ and $\tau = 1$, where the relaxation time τ aids in the determination of the viscosity of the fluid regardless of sample size, with convergence of the simulations obtained by using at least 2000 iterations. Idealised simulations of a cubic bed made up of spheres arranged in a 3×3×3 array showed that at low τ and low f_b, predicted values of U_s are likely to be constant. Using $f_b = 10^{-3}$ does affect the accuracy of predicted superficial velocities, and similarly when $\tau > 1$, with the impact of both these variables on U_s as shown in Fig. 8. All simulations were conducted using either a 64bit Windows Vista Ultimate OS running on 12Gb of DDR3 RAM, or for simulations larger than 400×400×600 in size, the University parallel computer Everest running on 8 processors using SuSE 10.0 OS.

The tests also investigated different locations within the overall packing from which the samples of differing dimensions were taken; namely from the bottom-middle, centre-middle and top-side of the larger bed. Considering results for the bottom-middle samples, not shown, both the constant length (600 LU) and constant cross-section (300 LU^2) sample results were

well behaved, with fixed length LBM predictions uniformly stable across the range of cross-sections examined ($k/S_d^2 = 2.84\times10^{-4}$-$3.08\times10^{-4}$). LBM predictions of k/S_d^2 with fixed cross-sectional area and increasing sample lengths showed that results stabilised by 300 LU, with small fluctuations thereafter ($k/S_d^2 = 2.58\times10^{-4}$-$2.84\times10^{-4}$). In general, the sample volumes exhibited little variability in porosity leading to a stable permeability. In addition, LBM predictions were in reasonable agreement with measured data and those obtained from the Carman-Kozeny equation.

Results for the centre-middle samples (Figs. 9 and 10) showed significantly more variability in the LBM predictions of permeability with sample size ($k/S_d^2 = 1.40\times10^{-4}$ -2.39×10^{-4}), and hence are considered in more detail here, with larger samples required than in the previous case to give converged results (typically 400×400×600 LU). In the case of the fixed length samples (Fig. 9), the rise in permeability with sample size closely mirrors results obtained from the Carman-Kozeny equation, although this is less noticeable in the results of Fig. 10. The requirement for a larger sample size is likely due to the random nature of the packed spheres in the case of samples taken from the centre of the bed. Samples taken from the bottom of the bed are therefore more likely to have retained some ordered structure due to the bed having been formed on a sieve filtration attachment within the filtration rig. In contrast, samples from the centre of the bed were approximately 200 sphere diameters above the base, with sphere packing being completely random by this point. For all the cases examined, including the results shown in Figs. 9 and 10, predictions of the Carman-Kozeny equation were not constant and were prone to fluctuate with sample size. This is caused by the difference in porosity from one sample to another, with smaller cross-section samples found likely to have porosities that vary most dramatically. Samples of 300 LU^3 had measured porosities in the range 0.262-0.416, whereas samples of 300×300×600 had a range of 0.356-0.368. In all cases, results obtained from the Carman-Kozeny equation also over-predicted the experimental data. Note that the experimental data shown in Figs. 9 and 10 are constant given that they were obtained for the bed as a whole at a single drive pressure of 1.5 bar.

[FIGURE 9]
[FIGURE 10]

Lastly, the top-side sample results, not shown, again showed a relatively high degree of k/S_d^2 variability with changing sample size (for fixed length = 2.7×10^{-4}-5.95×10^{-4}; for fixed cross-section = 2.81×10^{-4}-4.66×10^{-4}), although less than was observed for the case of centre-middle bed samples.

From an analysis of all the results, samples of dimensions of 300 LU^3 were generally acceptable in providing LBM predictions in line with experimental observation. Ideally, a cross-section of 400 LU^2 and a sample length of 600 LU (or greater) produces greater accuracy in the predictions, although at additional computational cost. Also, the difference in error between the LBM predictions and data found in the sensitivity studies due to the different bed sample locations at 1.5 bar was approximately 7%. This is considered to be acceptable and well within error margins. From these results there is therefore little to choose between the various samples taken from different bed locations. A bottom-middle sample, as previously noted, is more structurally ordered than those taken from elsewhere, being obtained from approximately 1 mm above the base of the bed, and hence likely to retain some end effects in terms of its internal structure. A centre-middle sample, in contrast, is likely to display random ordered packing due to its position within the packing matrix, with no end effects evident, but some influence from surrounding spheres. A top-side sample has the least ordered packing as these were taken from a location roughly 2 mm away from the top-edge of the bed, with the influence of any ordered packing from surrounding particles and wall effects reduced as a consequence. The predicted average porosity closest to the experimental value

was from the centre-middle sample, with a porosity of 0.351, compared with a measured value of 0.348, with the latter determined from:

$$\phi = \frac{(m_{ss} - m_{ds})V_{ds}}{\rho_w} \quad (8)$$

where m_{ss} and m_{ds} are the mass of saturated and dry sample, respectively, V_{ds} is the volume of dry sample and ρ_w the density of water.

A complete list of LBM predictions for the specific case of a drive pressure of 1.5 bar and bottom-middle samples is given in Table 2. This highlights the range of sample dimensions used to validate 400×400×600 pixels as a representative sample volume of the greater whole for glass beads of 116 μm (2μm/pixel resolution) in diameter.

[TABLE 2]

As a final point, it is worth commenting on the memory requirements of the LBM simulations. If large amounts of computing memory were available it would be feasible to undertake larger simulations, thus reducing the errors incurred from the size of bed sample employed. The type of RAM is also important as clock-speed determines the speed of the simulation iterations. Succi (2001) has previously illustrated how total memory requirements increase as grid size increases, with the present authors having observed a similar linear increase in the current work. Running large sample dimensions is therefore likely to decrease the error margins in the predictions, although computer costs in terms of RAM and run time are likely to render such calculations impractical in many situations.

3.2.2 Spherical particle beds

Glass beads are stable, simple geometric structures. How changes in pressure affect the permeability of different sample arrays was therefore first investigated for beds made up of such particles. Once knowledge of how bed structure relates to pressure in these simple geometric arrays is obtained, it should be possible to understand how more complex particle beds behave. From the sensitivity studies reported above, it can be assumed that an LBM prediction with dimensions 400×400×600 LU in Cartesian coordinates with, on average, 58.5 pixels used across the diameter of each particle is capable of giving reproducible results.

Figure 9 illustrates the superficial velocities predicted for samples taken from three regions of a larger bed for three different drive pressures. It illustrates how, as the drive pressure reduces, the superficial velocity decreases linearly with it. This confirms that the drive pressure can be translated accurately into a body force, and that a linear decrease in the body force is proportional to a linear decrease in the pressure.

[[FIGURE 11]

Once the mass flow rate was converted to a volume flow rate and subsequently to a velocity, the permeability was calculated using Eq. (1). Converting from a mass flow rate to a velocity is relatively simple, involving an average mass flow against time, the cross-sectional area of the pipe and the density of the fluid. Since experimental runs were repeated until a stable trend was noted, with a minimum of 7 runs in each case, an average mass flow rate was easily determined.

The permeability of a sample should not change significantly as long as that sample is homogeneous and uniform throughout, as confirmed by the results of Fig. 12, although some variability with the location from which the bed sample was taken is apparent. These results translate into those of Fig. 13 which demonstrates the difference between the average

permeability of a packed bed of glass beads obtained from experimental measurement and the average value calculated using the various digitally scanned sections taken from it.

[FIGURE 12]
[FIGURE 13]

The range in the results of Fig. 13 between the three pressures is low at 2%, with the minimum and maximum variation between the experimental and simulated results being 18.6% and 19.6%, respectively. This relatively narrow range is due to the homogeneity and uniform structure of spherical particle arrays.

Using the lattice Boltzmann method to predict the permeability of a packed bed of spherical particles under several pressures is therefore not only possible but leads to predictions in reasonable agreement with experimental data. With due care a sample with dimensions 400×400×600 LU, with a particle diameter represented using 16, but preferably 32, pixels, should give representative and reproducible results for simulations based on experimental bed samples. The use of 58.5 pixels across the diameter of the particles, as in this case, negated most, if not all, of the digitisation errors found in predictions using 32 pixels. This restricted the possibility for any errors between experimental data and predictions to be solely due to deviations in permeability measurements and the representativeness of bed samples, and not digitisation errors.

3.2.3 Sand particle beds

This section considers beds made up of mono-disperse polymorphous sand particles. The grains have a narrow size range, as seen in Fig. 14, and a mean diameter of 236μm. The aim in examining beds of such particles was to allow a transition between beds of fully homogeneous particles that are uniform in shape and structure, and those made up of completely inhomogeneous particles that are chaotic and do not relate to one another in terms of size or shape.

[FIGURE 14]

Due to the porosity and small size of the sand particle beds a drive pressure of 1.5 bar was found to be too great for examining flow through the bed. Our experimental setup used compressed air to push water through the filer cake formed within a small column, meaning the total volume was small. As such, depending on the added pressure, water was pushed through and exhausted over a short time span. Not only did high pressures force water through the bed extremely quickly, allowing only a few seconds of data to be recorded, but the force of the air directly onto the weigh scales following flow measurement led to erroneous results. The pressure was therefore decreased to reduce the flow rate through the bed, with values of 0.33, 0.67 and 1 bar used in these studies. This gave a more controlled flow through the bed and hence reliable results.

The sand particle bed simulations were run with a digital particle diameter of 24 pixels. Although significantly less than the 58.5 pixels used for the glass beads considered in the previous section, results derived on this basis were considered, from the studies reported in Section 3.1, to result in discretisation errors of an acceptable level. All the simulations were again undertaken using a body force $f_b = 10^{-4}$ and $\tau = 1$, as per the acceptable variable range noted in Section 3.2.1.

A sensitivity study was also undertaken to assess the minimum dimensions required to give a representative and reproducible sample of the larger sand particle bed. This study considered varying sample cross-sectional areas for a fixed sample length. For the case of a 600 LU length sample, predictions of the superficial velocity with varying cross-section are given in Fig. 15. Clearly there is a significant increase in U_s between 100 LU^2 and 118 LU^2, after

which stability is reached. There is a very large difference in sample volume between using 118 LU^2 and the largest cross-section examined, i.e. 400 LU^2. Despite this, however, the difference in superficial velocity between the two cases is negligible at 0.12%, although using the larger dimension is more likely to negate most if not all of any particle discretisation errors.

[FIGURE 15]

From the sensitivity study it was again accepted that LBM simulations with dimensions of 400×400×600 in lattice units gives an acceptable volume dimension to result in reproducible predictions. Figure 16 illustrates the superficial velocities predicted for samples again taken from three regions of the larger bed at the drive pressures noted above. A deviation of 4.3% between the highest and lowest porosity of these samples highlights the small differences between the structures of the bed in the three regions examined. The difference in porosity between the three sample zones can be considered minimal (0.397-0.415).

From earlier results and those of Fig. 16, the centre-middle sample is consistently of a lower velocity than its neighbouring samples for both glass beads and sand particles. However, the permeability for each bed type is not significantly different between the various sample locations. The difference lies in the range of porosity of the sampled areas. Whereas glass beads show the top-side sample as being, on average, the most permeable (Fig. 12), the beds of compressed sand particles show the bottom-middle sample as becoming the more porous with increasing superficial velocity (Fig. 17). These differences can, however, be considered minimal and part of the random and chaotic packing of any particle bed.

[FIGURE 16]
[FIGURE 17]

From Fig. 18, which compares the average permeability of the bed obtained from experimental measurement and the average value calculated using the digitally scanned sections taken from it, the range in the predicted permeability at different pressures is low at 2%, with an average error of 28.8% between measurements and predictions of permeability. This emphasises that the individual permeabilities between sample zones and pressures are mostly well behaved, and it is reasonable to assume that the relatively small differences are due to the homogeneity of the sand particles. Although less uniform in shape than spheres, therefore, it is not the sphericity of the particles that determines a uniform bed porosity, which encourages uniform flow through the bed, but how greatly particles deviate from their bulk average geometry. Although sand particles are not geometrically identical to one another, they do have sufficient geometric similarity to be considered analogous. Compared with glass spheres, although the accuracy of the LBM predictions fell (19.2% versus 28.8%) when predicting sand particles, the qualitative similarities are obvious. Both types of particle confirm that the centre-middle sample is more densely packed than the top-side and bottom-middle samples. Both particle types also have a near consistent deviation between predictions obtained using samples from different bed locations, and both particle types validate the feasibility of using small samples of a bed to predict the bulk properties of the bed as a whole.

[FIGURE 18]

Due to the less uniform geometry of sand particles it is understandable that, to some extent, the permeabilities of individual sections of bed vary more than for the case of uniform glass beads. Using the lattice Boltzmann method to predict the permeability of a packed bed of sand particles under several pressures, as described, is however feasible, and gives stable results. As mentioned in the case of glass beads, with due care a section of a bed, scanned and with the dimensions noted across each axis, can be represented using greater than 16 pixels across a particle diameter to give representative and reproducible predictions of bed

permeability. The results also indicate that although predicting the flow characteristics of a bed from a single sample at a single pressure is possible, with a certain degree of error, it is not advisable. Indeed, we advocate taking the average of the predictions from different locations of the bed as this provides a better overall estimate of permeability, especially for heterogeneous packing. Due to the packed beds of glass spheres, and to a lesser extent the sand particles, being homogenous in structure it is not unreasonable to assume that averaging the superficial velocities across all beds is an adequate method of data amalgamation. As complexity of the bed increases homogeneity of the bed falls and simple averaging of the various samples may not be adequate. However, by utilising the approach presented, it is possible for one to identify the varied, or be it uniform, nature of the materials at hand, and therefore make an informed decision as whether to use a single sample or to obtain an average from numerous bed locations.

3.2.4 Polydisperse, polymorphous particle beds

Beds made up of mixtures of polydisperse and polymorphous particles are considered below in order to establish whether it is possible to simulate flow through the chaotic structure of a porous bed of six different materials. As noted earlier, most previous research assumes particles within a bed to be spherical, or uniform in shape, although such assumptions are not possible for the beds considered here. This section uses LBM to predict the flow through a purely random bed containing a haphazard collection of particles ranging from 115μm to 375μm in length.

Unlike the previous sections, complicated particle geometries and bed structures are considered. The particles were made up of six different types of common minerals, namely gypsum, kyanite, mica, hornblende and garnet plus silica sand, which were ground using a pestle and mortar and sieved to give a controlled range of particle sizes. The reason for using different minerals was due to their geometric properties. When ground the mineral particles retain their geometric shape thereby producing a range of geometries (bladed, spherical, needle, rectangular and abstract shapes) for packing, instead of being ground to amorphous or rounded particles, as shown in the microscopic images of Fig. 19.

[FIGURE 19]

A sensitivity study was again performed to ensure reproducible predictions and to minimise discretisation errors to an acceptable level. To minimise the discretisation error in a simulation it has been found that, for spherical and near-spherical particles, a minimum of 16 pixels across the particle length is required. However, for particles that are far from spherical in shape the average number of pixels per particle is difficult to estimate due to the varied shape of the particles together with their varied sizes within a bed. The solution used here was to establish an average value for the particles considered. Assuming the range of particles was equally distributed, i.e. the number of particles of 115μm length was similar to the number of particles of 375μm, then a representative average is the difference in size between the largest and smallest particles divided by the pixel resolution. If P_{avg} is the average particle size, therefore, $S_{m,max}$ and $S_{m,min}$ are the maximum and minimum sieve mesh sizes, respectively, and R_p is the pixel resolution from the XMT scan, then:

$$P_{avg} = \frac{S_{m,max} - S_{m,min}}{R_p} \tag{9}$$

Using this approach the average particle length was determined as 52 LU, with this resolution used in subsequent simulations.

Figure 20 gives results for the superficial velocity obtained using a fixed length sample of 600 LU and varying cross-section, with the sample taken from the top-side of the bed (and with

similar results found for other sample locations). All the simulations were again undertaken using a body force $f_b = 10^{-4}$ and $\tau = 1$, as per the acceptable variable range noted in Section 3.2.1. These results show that a cross-section of 240×240 lattice units is not likely to give representative predictions, whereas results obtained using a value of 288×288 are much closer to the constant superficial velocity achieved at higher cross-sectional values. This study therefore confirmed that the use of a sample of 400×400×600 LU, as employed in determining the results given below, was suitable for simulating beds made up of particles with an average length of 52 LU.

[FIGURE 20]

The varied size and shaped particles created a bed that was geometrically complex and thoroughly inhomogenous. A drive pressure of 1 bar was found to be too high to measure flow through the bed accurately in the experimental study, and therefore reduced pressures of 0.25, 0.5 and 0.75 bar were employed in the study of this particular bed.

Figure 21 again shows that, for each bed sample location, a linear increase in the superficial velocity accompanies an increase in pressure. The straightness of each line confirms that variations in results between sample locations were not due to human error, with the differences stemming inherently from low pressures, although they increase significantly with pressure. These variations in gradient were largely due to differences in the porosity of the bed which, even though attempts were made to ensure that inter-particle adhesion was kept constant throughout the bed, were caused by stratification of the different particle types. Closer examination of the bed therefore showed that a layering effect had, to some extent, occurred during its formation, with the heaviest particles settling first. Needle-like particles then layered in the middle of the bed while the lighter particles tended to rest on top of the needle-like particles. The intertwining of the needles was also found to allow large pore spaces to form, thereby increasing the porosity (0.538) of that section of the bed regardless of the compressive nature of the pressure and flow through it. This compares with porosities of 0.376 and 0.385 for bottom-middle and top-side samples, respectively. The results of Fig. 21 reflect this finding, where the centre-middle sample is seen to show superficial velocities in excess of those found for samples from other locations. Results for the predicted permeability are given in Fig. 22, and these again reflect the nature of the bed examined. Unlike experimentally measured permeabilities, considered further below, the simulated values remain relatively constant with pressure for each sample location, with differences between the various samples in line with expectation, and with the centre-middle sample deviating significantly from the other bed sample locations.

[FIGURE 21]
[FIGURE 22]

Figure 23 compares experimental data and predictions of the average bed permeability. Given the complexity of this bed, there is surprisingly little error between the two. These results are to some extent misleading, with the results for beds of both glass and sand particles showing a significantly higher error between prediction and experiment than for the bed considered here. In terms of the predictions, LBM is not morphologically sensitive, so that although spherical and near-spherical particles are simple to represent, that does not make flow through beds of such particles simpler to predict than in the present case. What should be noted is that the inherent error in performing experiments with polydisperse and polymorphous particles was increased significantly due to the use of sieves rather than the Mastersizer for particle size measurements. Overall, therefore, the error in permeability data obtained for the simpler beds was assessed to be of the order of 17%, whereas for the bed considered here that value increased to about 25%. Hence, although the difference between measurements and predictions may be low in the present case, including inherent errors gives deviations between

the two of the same order of magnitude as for the other bed types considered. Also worthy of note is that the error in the pressure measurements increased significantly with decreasing pressure. Again, these errors were assessed to be of the order of 1-2% over the range of pressures used in the case of the simpler beds, whilst for the bed of polydisperse and polymorphous particles this increased to around 14% due to the lower head of water used in these experiments and the increasing influence of gravity on the results.

[FIGURE 23]

Use of LBM to predict the permeability of an inhomogeneous bed of polymorphous and polydisperse particles at several pressures would therefore appear possible. However, unlike for the previous simpler beds where a single sample volume was sufficient to yield reasonably accurate predictions of permeability, in the case of beds with highly complex, inhomogeneous structures samples from across the entire bed are required to yield averages that account for any stratification of particles within the bed. Individual samples from such beds therefore differ significantly in terms of their porosity, which in turn has a significant impact on predictions of superficial velocity and permeability. Average particle lengths in the bed examined ranged from 115μm to 375μm, and calculating a representative average particle size is important. This study used one approach to determine a representative average, although other approaches are possible and worthy of further investigation.

The primary interest in this work was in 'trend' rather than absolute values. Hence, the use of lattice units (LU^2) to express permeability (where one lattice unit (LU) is equal to one voxel), as opposed to physical length measurements (of m^2). The main reason for this was to simplify relating the XMT data to LBM dimensionless units. However, the ultimate aim of the application is to predict the permeability of materials of interest and to present them in SI units. To convert LU to m, one uses pixel width (m/pixel), which in the reported predictions was $2x10^{-6}$m/pixel. The real value (m^2) of the averaged permeability, for mono-sized sphere-packed beds with an individual particle diameter of 58 pixels (116μm @ 2μm/pixel resolution) varied between 6.87E-10 m^2 (0.5bar) and 6.94E-10 m^2 (1.5bar). The permeability within the sample does not change significantly provided that sample is homogenous.

4. Conclusions

The aim of the work described has been to create the foundations for the development of a virtual permeameter that would enable the structure-flow relationships for bulk porous media to be assessed entirely using numerical methods. The feasibility of such an approach was explored on the basis of small samples taken from larger packed beds, with X-ray micro-tomography employed to image the samples for use as input to subsequent LBM calculations. The rationale behind this was to reduce the requirement for expensive and repetitive experiments needed to assess the effectiveness of packed beds currently used within industries where filtration is an important part of their processes. The final step in the development of a virtual permeameter is to replace the need for X-ray micro-tomography scans of actual bed samples by a digital particle packing algorithm (Jia and Williams, 2001) which would be used to construct digital representations of a bed and hence provide input to the LBM calculations, although that is beyond the scope of the present work.

It has been determined that simulations of flow through a packed bed, regardless of particle morphology and heterogeneity, are capable of being accurately predicted using the lattice Boltzmann method.

For beds of spherical and near-spherical particles, it has been shown that permeability predictions converge at a resolution of approximately 16 pixels across the diameter of the particles, with acceptable differences from results obtained using much higher resolutions.

Resolutions equal to or greater than this ensure that any deviations in results between experiments and XMT/LBM simulations performed to determine the permeability of a packed bed are unrelated to discretisation errors. The required dimensions of a sample needed to allow accurate prediction of flow through such beds, and the bed permeability, was found to be of the order of 300×300 pixels in cross-section and 300 pixels in length. Provided that the bed particles are adequately resolved within a simulation, and the bed sample is above the specified size, it is concluded that, for the beds of spherical and near-spherical particles considered, any bed sample is capable of providing reproducible simulation results, irrespective of the section of the bed from which it is obtained. Permeability predictions are on average within 19% and 29% of measured data for spherical and non-spherical particle beds, respectively.

For more complex packed beds of polymorphous, polydisperse particles it has been found that a significantly greater variability exists between samples taken from different bed locations. It was therefore established that a single sample was not sufficient to account for stratification of particles within a packed bed of non-homogeneous particles. For this reason, an average of the packed bed sample sections must be used to produce representative results.

References

Adler PM. Fractal porous media III: Transversal Stokes flow through random and Sierpinski carpets. Transport in Porous Media 1983;3:185-198.

Aidun CK, Lu Y. Lattice Boltzmann simulation of solid particles suspended in fluid. J Statistical Physics 1995;81: 49-61.

Arns CH, Knackstedt MA, Pinczewski VW, Martys NS. Virtual permeametry on microtomographic images. J Petroleum Sci and Eng 2004;45:41-6.

Bhatnagar PL, Gross EP, Krook M. A model for collision processes in gases. I. Small amplitude processes in charged and neutral one-component systems. Phys Rev 1954; 94:511-25.

Caulkin R, Jia X, Fairweather M, Williams RA. Lattice approaches to packed column simulations. Particuology 2008;6:404-11.

Clague D, Phillips R. A numerical calculation of the hydraulic permeability of three-dimensional disordered fibrous media. Physics of Fluids 1997;9:1562-72.

Dünweg B, Ladd AJC. Lattice Boltzman simulations of soft matter systems. Adv Comp Sim Approaches for Soft Matter Sci III, Adv Polymer Sci 2009;221:89-166. Springer-Verlag Berlin Heidelberg 2008.

Jia X, Williams RA. A packing algorithm for particles of arbitrary shapes. Powder Tech 2001;120:175-86.

Klemm A, Kimmich R, Weber M. Flow through percolation clusters: NMR velocity mapping and numerical simulation study. Phys Rev E 2001;63:041514.

Koch DL, Hill RJ, Sangani AS. Brinkman screening and the covariance of the fluid velocity in fixed beds. Physics of Fluids 1998;10:3035-37.

Macnab A, Vahala G, Vahala L, Pavlo P. Lattice Boltzmann model for dissipative MHD. In: Proceedings 29th EPS conference on controlled fusion and plasma physics. Montreux, Switzerland, June 17-21; 2002. Vol 26B.

Martys NS, Chen H. Simulation of multicomponent fluids in complex three-dimensional geometries by the lattice Boltzmann method. Phys Rev E 1995;53:743-51.

McCabe WL, Smith JC, Harriot P. Unit operations of chemical engineering. 7th ed. New York: McGraw-Hill; 2005.

Muhammad S. New models for natural and hydraulic fracturing of heterogeneous rock. Soc Petroleum Eng, SPE western regional meeting, Bakersfield, California. March 8-10, 1995.

Qian YH, D'Humieres D, Lallemand P. Lattice BGK models for Navier-Stokes equation. Europhys Letters 1992;17:479-84.

Stanley HE, Andrade Jr, JS. Physics of the cigarette lighter: Fluid flow through structures with randomly-placed obstacles. Physica A 2001;295:17-30.

Stockman HW. A 3D lattice Boltzmann code for modelling flow and multi-component dispersion. Sandia Report, SAND99-0162, 1999.

Succi S. The lattice Boltzmann equation for fluid dynamics and beyond. Oxford: Clarendon Press; 2001.

Sullivan SP, Akpa BS, Matthews SM, Fisher AC, Gladden LF, Johns ML. Simulation of miscible diffusive mixing in microchannels. Sensors and Actuators B 2007;123:1142-52.

Tafreshi HV, Rahman MSA, Jaganathan S, Wang Q, Pourdeyhimi A. Analytical expressions for predicting permeability of bimodal fibrous porous media. Chem Eng Sci 2009;64:1154-59.

Thies-Weese DME, Phillipse AP. Liquid permeation of bi-disperse colloidal hard-sphere packings and the Kozeny-Carman scaling relation. J Colloid and Interface Sci 2004;162:470-80.

Vidal D, Ridgway C, Pianet G, Schoelkopf J, Roy R, Bertrand F. Effect of particle size distribution and packing compression on fluid permeability as predicted by lattice-Boltzmann simulations. Comp and Chem Eng 2009;33:256-66.

Wildenschild D, Hopmans JW, Vaz CMP, Rivers ML, Rikard D, Christensen BSB. Using X-ray computed tomography in hydrology: System, resolutions, and limitations. J Hydrology 2002;267:285-97.

Wolf-Gladrow DA. Lattice-gas cellular automata and lattice Boltzmann models. Berlin: Springer; 2000.

Zamani A, Maini B. Flow of dispersed particles through porous media – deep bed filtration. J Petroleum Sci & Eng 2009;69:71-88.

Tables

Sphere Diameter (pixels)	Permeability (k/S_d^2)	Relative error to asymptote value (%)
2	16.86	80.56
4	69.33	20.09
8	64.13	26.08
16	74.18	14.49
32	81.55	6.01
64	85.63	1.30
128	86.76	0

Table 1. Comparison of relative permeability error arising from pixilation of spherical particles.

Dimension / LU	U_s / LU δt^{-1}	Re	k / LU^2	k/S_d^2
100×100×100	6.21×10^{-4}	0.218	1.036	3.03×10^{-4}
100×100×200	7.93×10^{-4}	0.278	1.322	3.86×10^{-4}
100×100×300	6.79×10^{-4}	0.238	1.132	3.31×10^{-4}
100×100×400	5.95×10^{-4}	0.209	0.991	2.90×10^{-4}
100×100×600	6.24×10^{-4}	0.219	1.040	3.04×10^{-4}
200×200×200	4.74×10^{-4}	0.166	0.790	2.31×10^{-4}
200×200×300	5.12×10^{-4}	0.180	0.854	2.50×10^{-4}
200×200×400	4.55×10^{-4}	0.160	0.759	2.22×10^{-4}
200×200×600	6.11×10^{-4}	0.214	1.018	2.97×10^{-4}
300×300×300	5.35×10^{-4}	0.188	0.891	2.60×10^{-4}
300×300×400	5.29×10^{-4}	0.186	0.882	2.58×10^{-4}
300×300×600	5.84×10^{-4}	0.205	0.973	2.84×10^{-4}
400×400×600	6.33×10^{-4}	0.222	1.055	3.08×10^{-4}
600×600×600	6.31×10^{-4}	0.221	1.052	3.07×10^{-4}

Table ~~1~~2

Table 2. Variation of LBM predictions of flow through a packed bed of glass beads at a drive pressure of 1.5 bar with sample size.

Figures

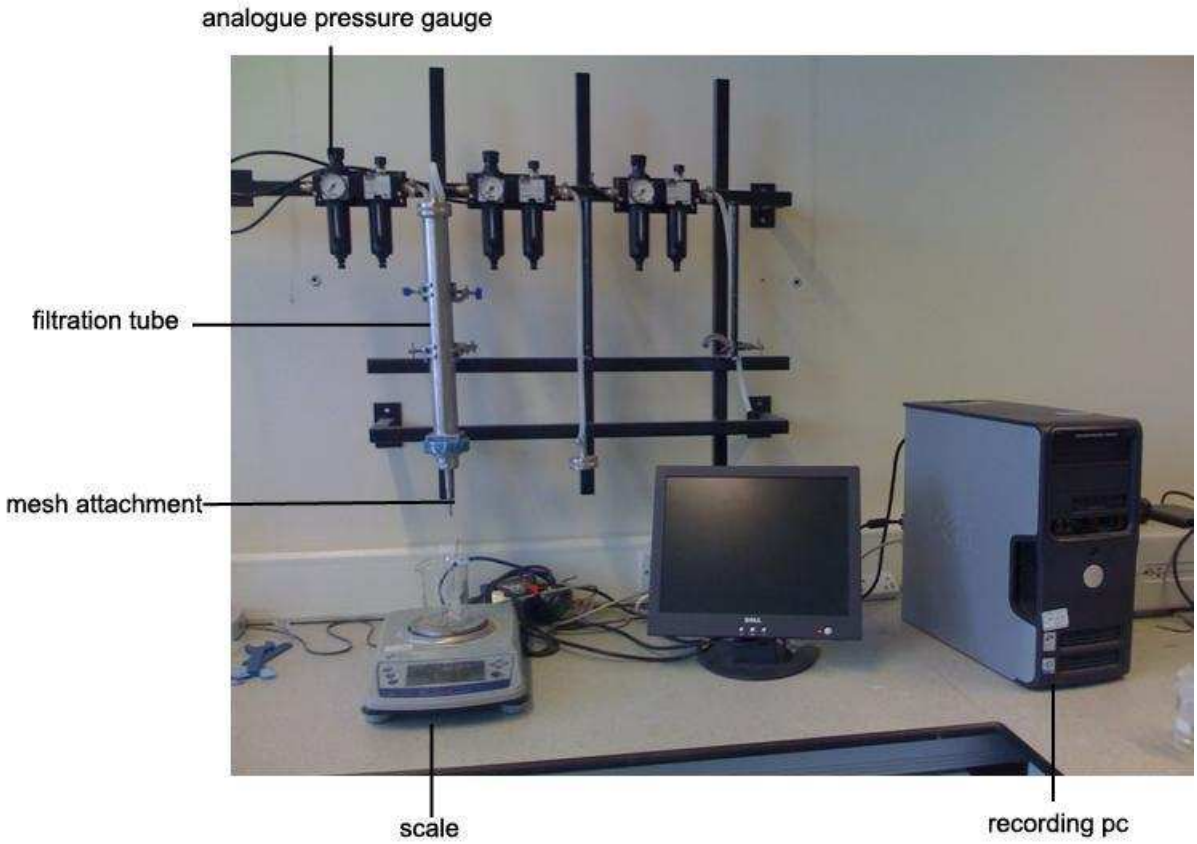

Figure 1

Figure 2

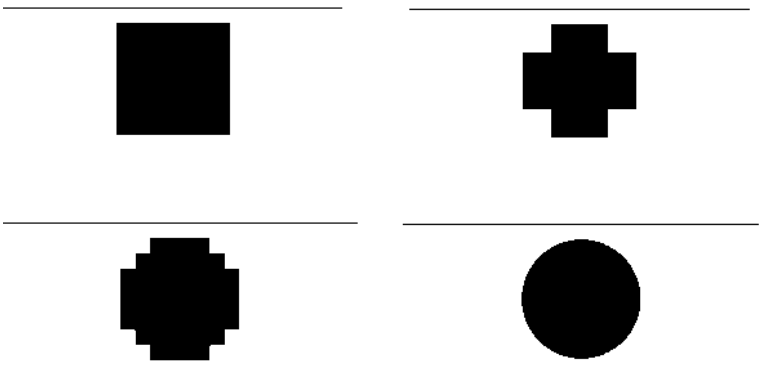

Figure 3

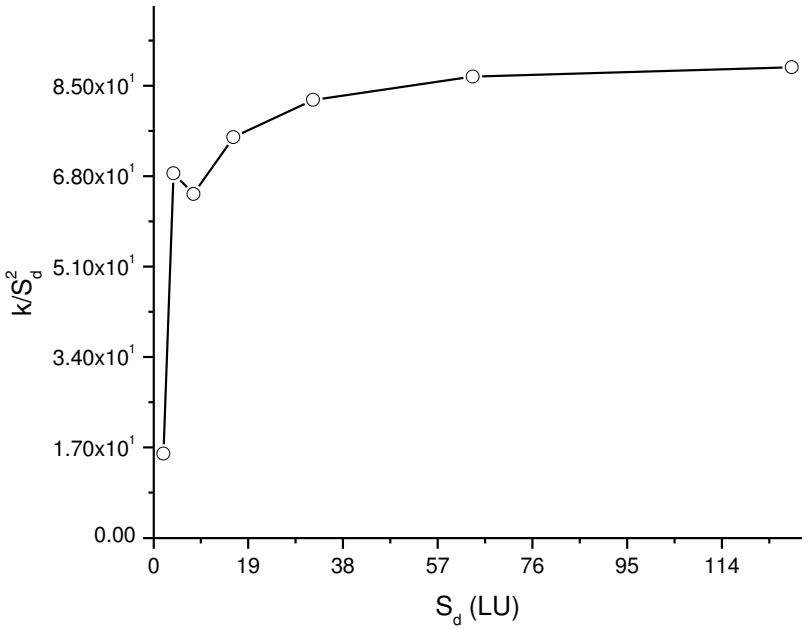

Figure 4

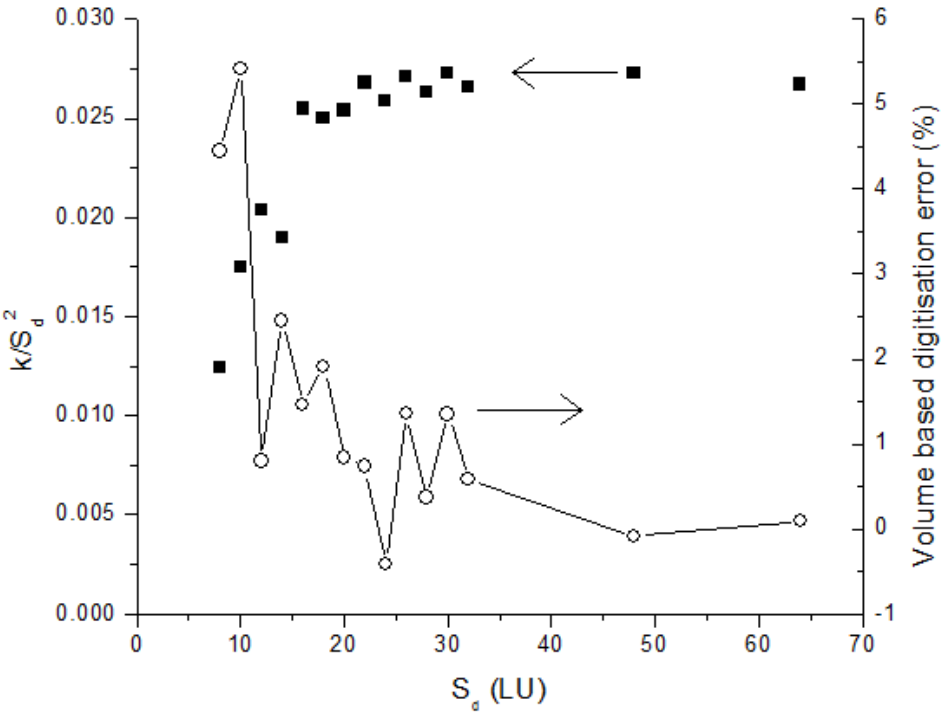

Figure 5

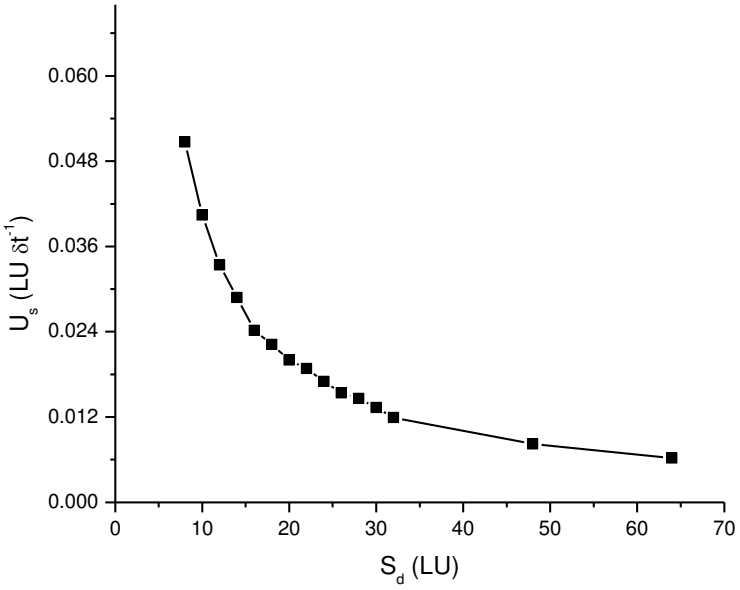

Figure 6

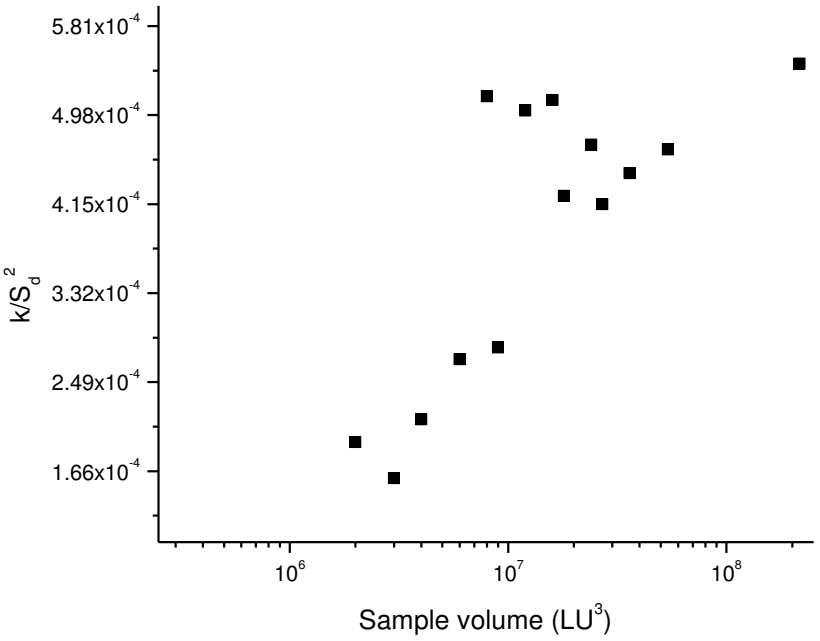

Figure 7

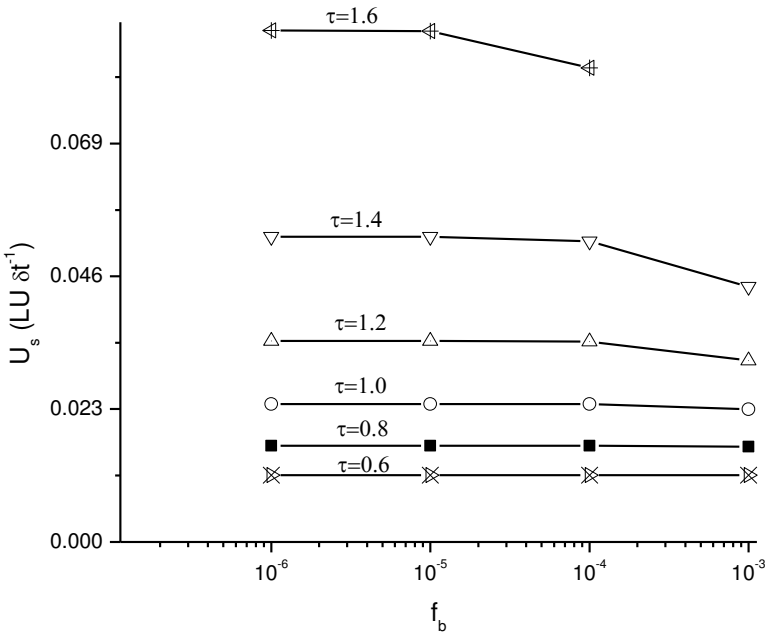

Figure 8

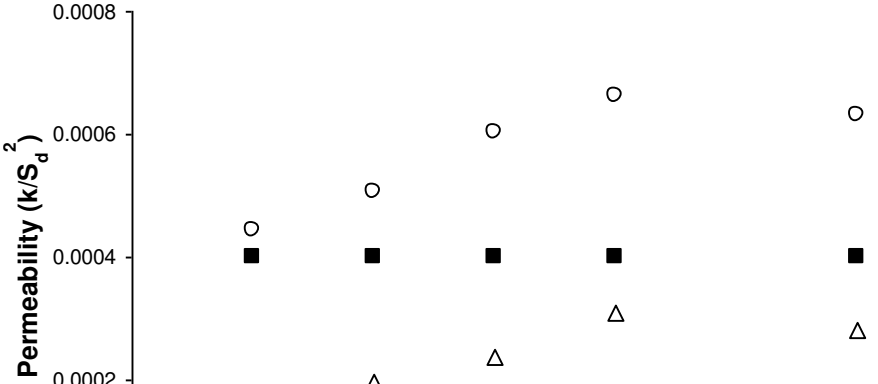

Figure 9

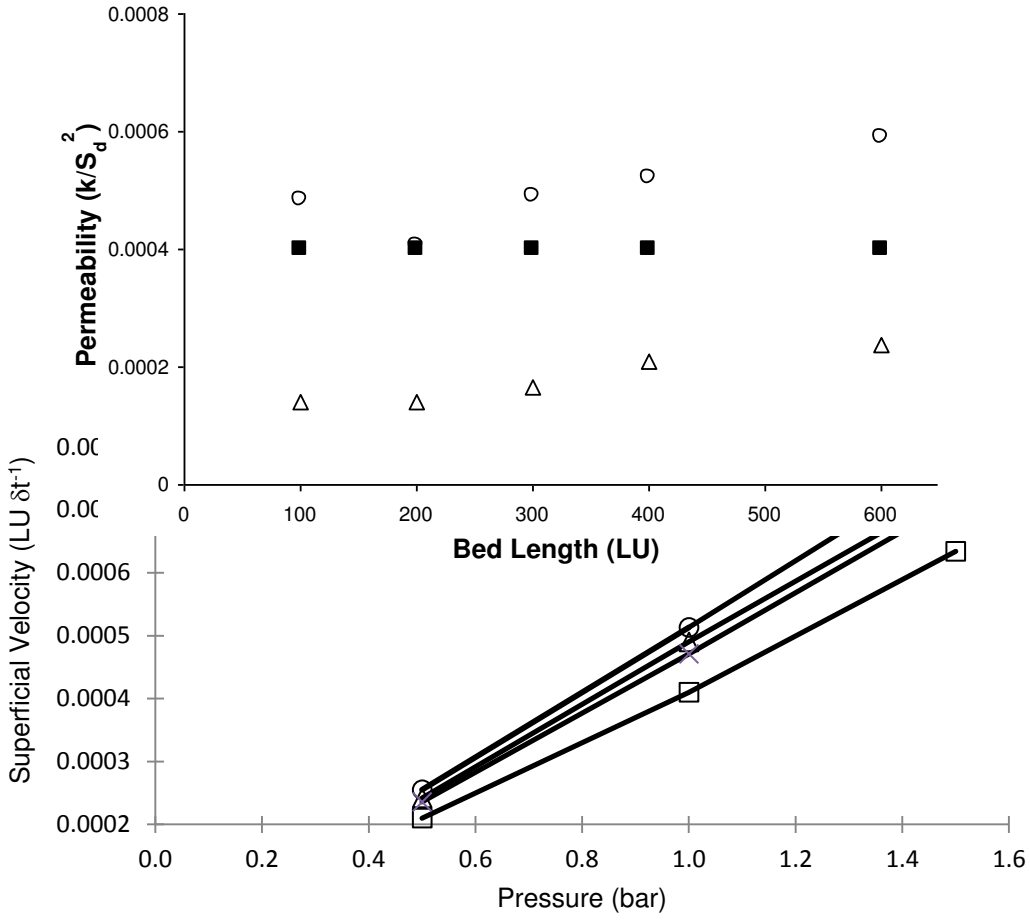

Figure 11

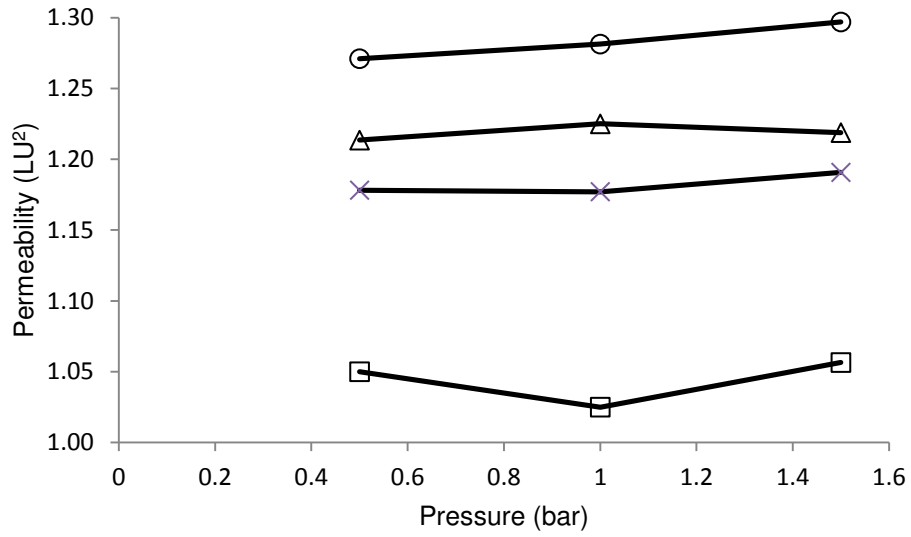

Figure 12

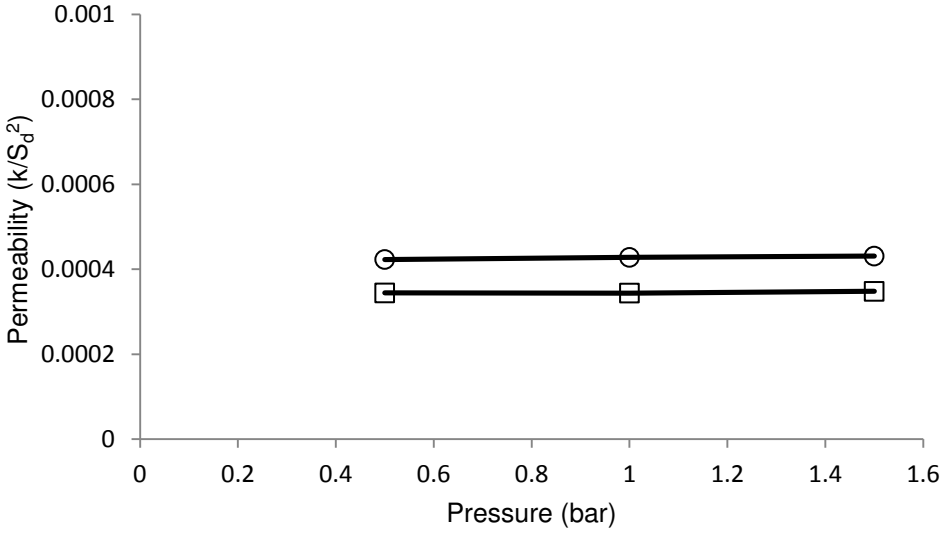

Figure 13

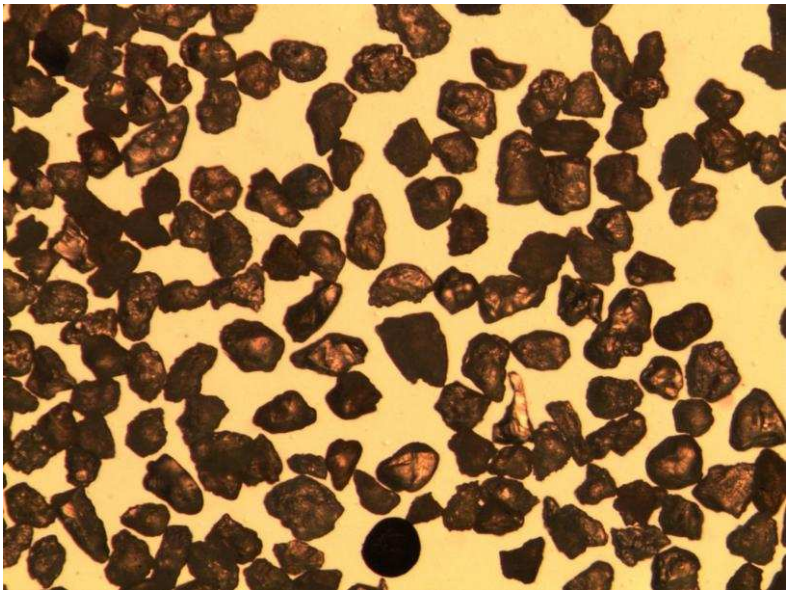

Figure 14

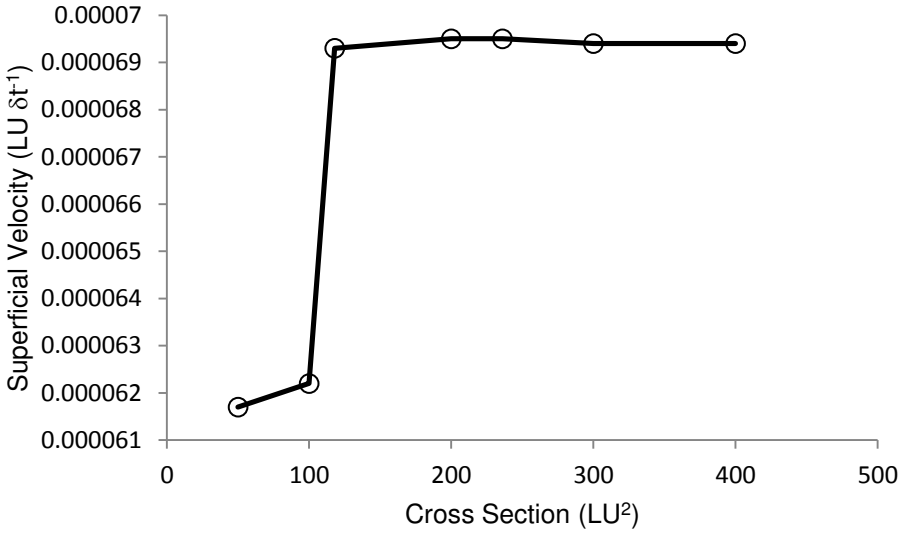

Figure 15

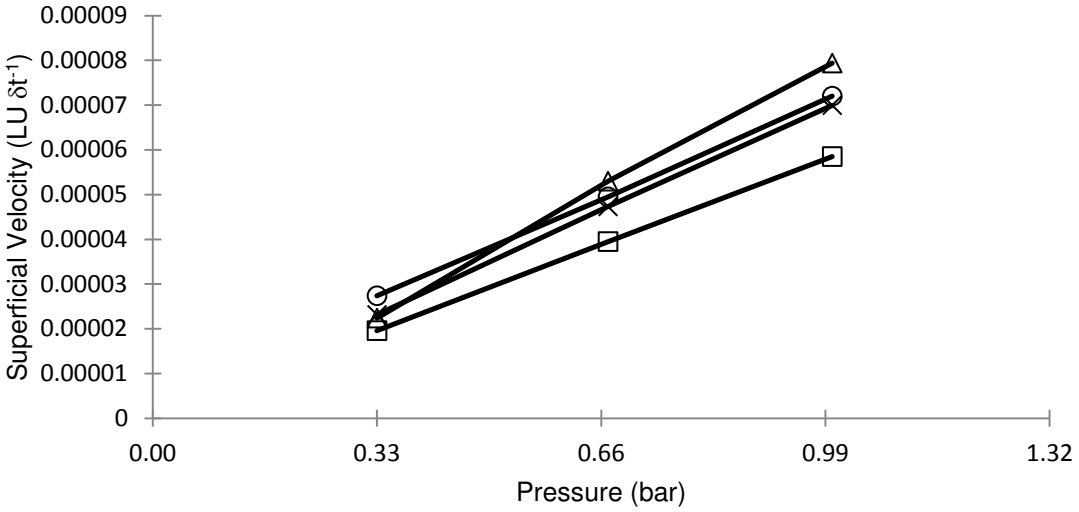

Figure 16

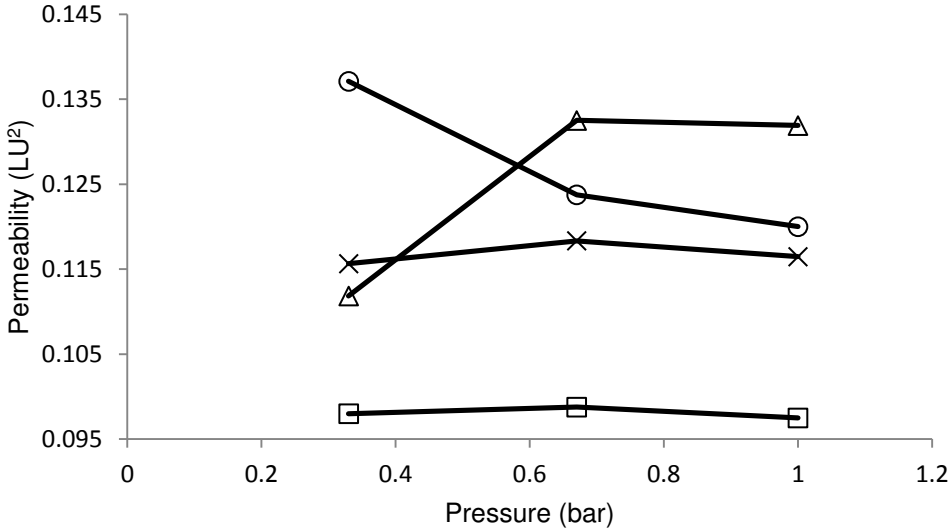

Figure 17

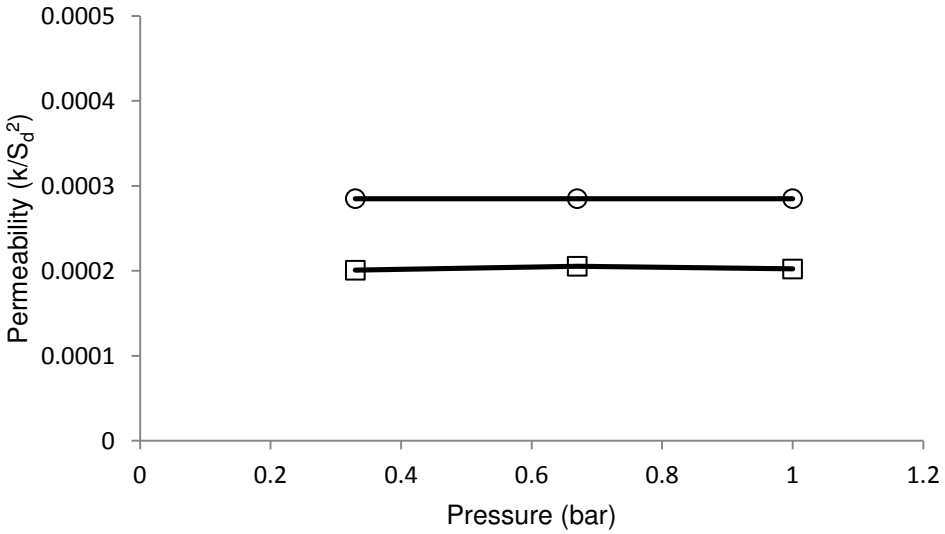

Figure 18

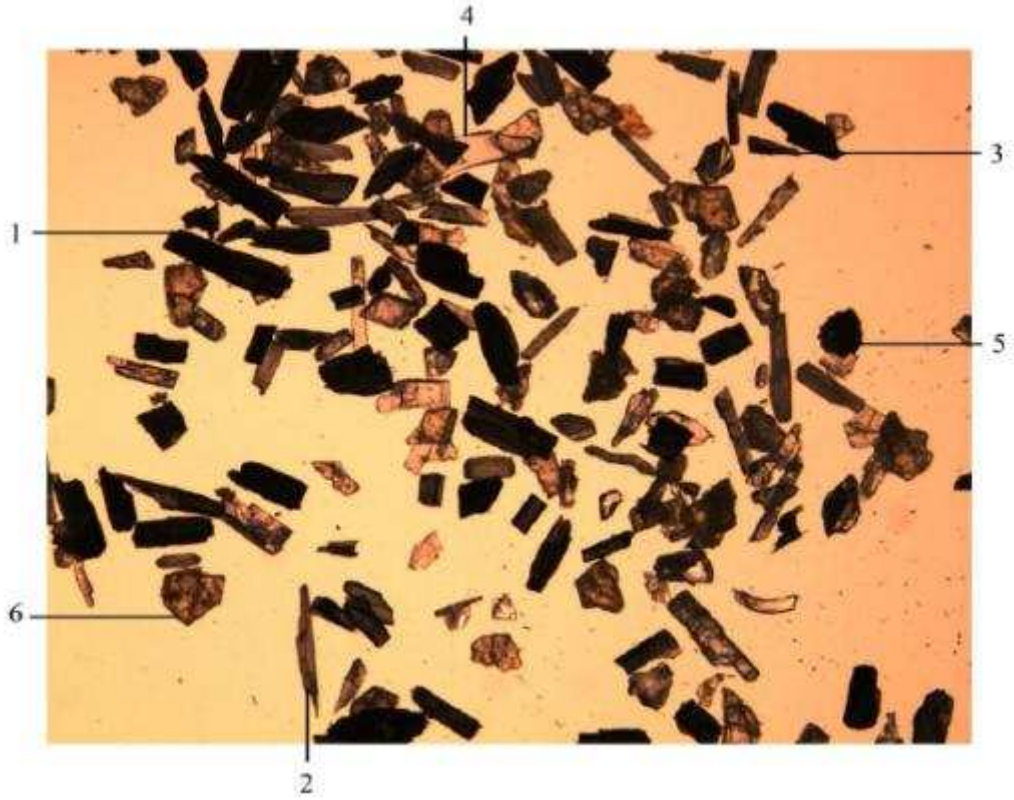

Figure 19

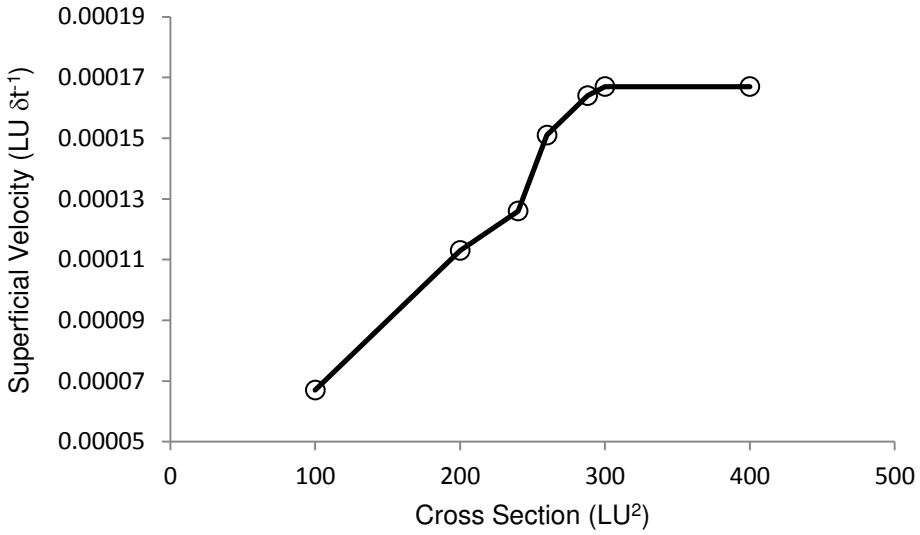

Figure 20

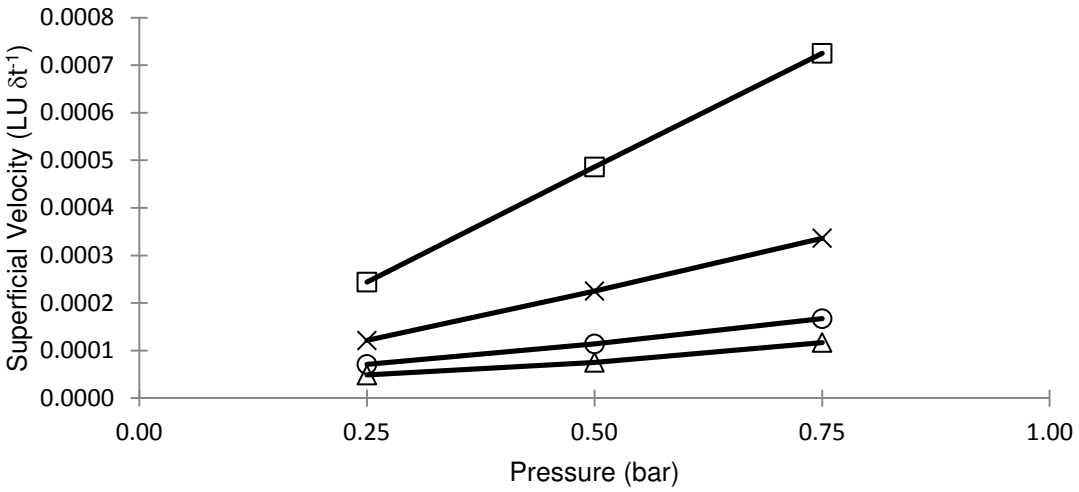

Figure 21

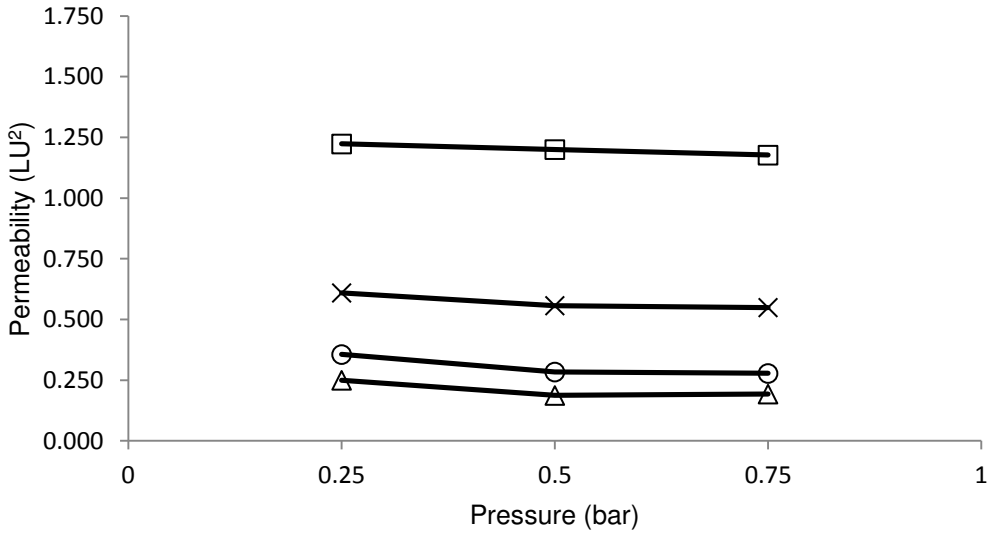

Figure 22

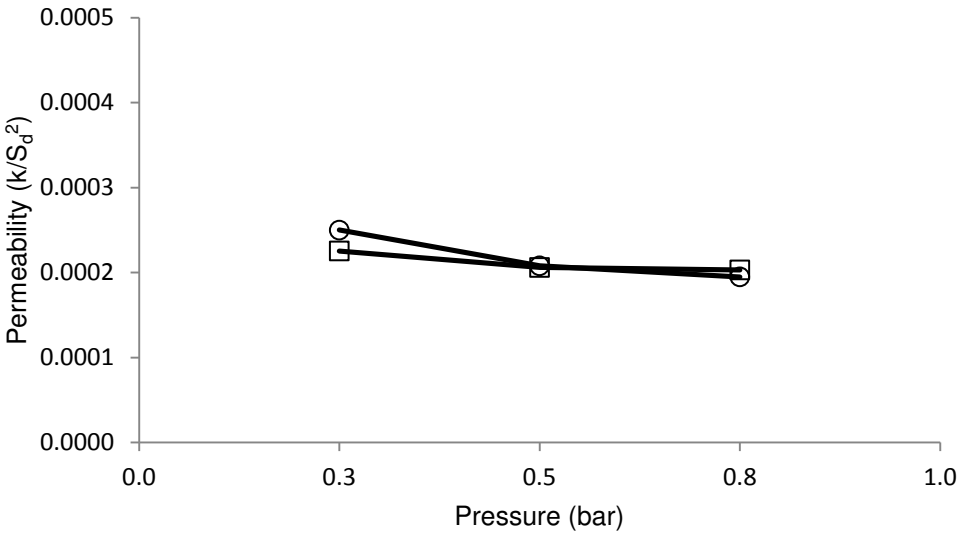

Figure 23

Figure Captions

Figure 1. The experimental setup: Analogue gauges attached to a steel filtration tube with a mesh attachment. The flow is measured as a function of weight against time and recorded by the computer. Data is then converted from a mass to a velocity flow rate.

Figure 2. (Clockwise from top-left): A whole packed bed of glass beads, how the samples were cut, two individual samples cut from the packed bed (each approx. $8mm^3$) and a x20 magnification of a sample cutting.

Figure 3. Visual representation of digitised spheres with diameters of 2, 4, 8 and 128 pixels.

Figure 4. Variation of permeability as a function of the accuracy of the digital representation of a sphere for flow in a duct with constant wall effects.

Figure 5. Variation of permeability and particle volume relative to a perfect sphere as a function of the accuracy of the digital representation of a sphere for flow in a duct with variable wall effects.

Figure 6. Variation of superficial velocity as a function of the accuracy of the digital representation of a sphere for flow in a duct with variable wall effects.

Figure 7. Variation of permeability as a function of sample volume.

Figure 8. Simulation stability for calculations using a 3×3×3 array of spheres as a function of relaxation time and body force.

Figure 9. Variation of permeability with size of fixed length samples taken from centre-middle of bed (■ – data, △ – LBM, ○ – Carman-Kozeny equation).

Figure 10. Variation of permeability with size of fixed cross-section samples taken from centre-middle of bed (■ – data, △ – LBM, ○ – Carman-Kozeny equation).

Figure 11. Variation of predicted superficial velocity with pressure for samples from a bed of spherical particles (○ top-side, □ centre-middle, Δ bottom-middle, × average).

Figure 12. Variation of predicted permeability with pressure for samples from a bed of spherical particles (○ top-side, □ centre-middle, Δ bottom-middle, × average).

Figure 13. Variation of experimental and simulated dimensionless permeability with pressure (○ experimental, □ simulated).

Figure 14. A ×30 magnification of sand particles. Note that the majority of particles are similar in size but dissimilar in shape.

Figure 15. Variation of superficial velocity with size of fixed length samples.

Figure 16. Variation of predicted superficial velocity with pressure for samples from a bed of sand particles (○ top-side, □ centre-middle, Δ bottom-middle, × average).

Figure 17. Variation of predicted permeability with pressure for samples from a bed of sand particles (○ top-side, □ centre-middle, Δ bottom-middle, × average).

Figure 18. Variation of experimental and simulated dimensionless permeability with pressure (○ experimental, □ simulated).

Figure 19. Microscope image (×10 magnification) showing geometric properties of ground mineral fragments (1 gypsum, 2 kyanite, 3 mica, 4 horneblende, 5 garnet, and 6 silica sand).

Figure 20. Variation of superficial velocity with size of fixed length samples.

Figure 21. Variation of predicted superficial velocity with pressure for samples from a bed of polydisperse, polymorphous particles (○ top-side, □ centre-middle, Δ bottom-middle, × average).

Figure 22. Variation of predicted permeability with pressure for samples from a bed of polydisperse, polymorphous particles (○ top-side, □ centre-middle, Δ bottom-middle, × average).

Figure 23. Variation of experimental and simulated dimensionless permeability with pressure (○ experimental, □ simulated).